Exciton formation in graphene bilayer

Raoul Dillenschneider[1,*] and Jung Hoon Han[2,3,†]
[1]*Department of Physics, University of Augsburg, D-86135 Augsburg, Germany*
[2]*Department of Physics, BK21 Physics Research Division, Sungkyunkwan University, Suwon 440-746, Republic of Korea*
[3]*CSCMR, Seoul National University, Seoul 151-747, Republic of Korea*
(Received 19 September 2007; revised manuscript received 4 March 2008; published 1 July 2008)

Exciton instability in graphene bilayer systems is studied in the case of a short-ranged Coulomb interaction and a finite voltage difference between the layers. Self-consistent exciton gap equations are derived and solved numerically and analytically under controlled approximation. We obtain that a critical strength of the Coulomb interaction exists for the formation of excitons. The critical strength depends on the amount of voltage difference between the layers and on the interlayer hopping parameter.

DOI: 10.1103/PhysRevB.78.045401 PACS number(s): 71.35.−y, 71.20.Mq, 78.67.Pt

I. INTRODUCTION

Graphene, layers of two-dimensional honeycomb array of carbon atoms, has attracted much interest these last few years due to its recent experimental accessibility[1–3] and a wide variety of interesting properties.[4–6] Both the single-layer and the multilayer graphenes are studied intensely. Much of the peculiar properties of the graphene layers arise from the energy spectrum near the so-called Dirac nodal points and the nontrivial topological structure of the wave functions around them.[1,7]

As the engineering application of the graphene layers attracts increasing significance, we need to explore, experimentally and theoretically, ways to enrich graphene's electrical properties and to control them. One way to achieve some control over the electrical properties is to change the number of layers and/or the bias applied across the layers. A recent experimental realization of the biased graphene bilayer is such an example.[8–10] By applying a gate bias across the two-layered graphene, the authors of Refs. 8 and 10 have observed a tunable energy gap varying with the bias (see Fig. 1 for the bilayer graphene energy bands in the presence of bias). The bias can also potentially control the formation of excitons. Since the applied bias leads to the charge imbalance in the two layers, it is natural to suspect that the Coulomb attraction of the excess electrons and holes on opposite layers would lead to an exciton instability similar to the situations considered in an earlier literature.[11–13] If so, it will provide an additional control over the graphene as the formation of excitons is known to affect the electrical properties significantly.[12,14]

Recent works on the exciton instability in a single-layer graphene are based on the Dirac Hamiltonian description.[15,16] The exciton gap is derived and solved through a self-consistent equation similar to the one appearing in the chiral symmetry-breaking phenomenon.[17] It was shown that an exciton can be formed under a strong long-ranged particle-hole interaction.[18] Exciton can also be formed in a single-layer graphene through the mechanism of magnetic catalysis of dynamical mass generation, as pointed out in Ref. 19. This work showed that the magnetic catalysis can induce exciton condensation even for weak particle-hole coupling.[20,21] These results are obtained in the framework of quantum electrodynamics (QED) deduced from the linear energy spectrum of the graphene monolayer.

In the case of a bilayer, additional excitonic channels become possible as the excess electrons and holes from the two layers can form a "real-space" exciton. In this paper, we consider the possibility of an excitonic instability in the biased graphene bilayer in the framework of Hartree-Fock theory. A conventional Hartree-Fock treatment had been used in the past to understand the exciton formation in semiconductors with success.[14] It is shown that the exciton can be formed if the strength of the Coulomb interaction U is larger than the threshold value U_c, which, for realistic graphene parameters, is comparable to the intralayer hopping energy. The threshold U_c is, in turn, bias dependent and can be tuned to a minimum value for an optimal bias V_o. Moreover, a reduction of the interlayer hopping, perhaps through intercalation, is shown to greatly reduce the threshold value U_c.

In identifying excitonic channels, we consider two possible scenarios. One is the pairing through the shortest-distance neighbors between the layers (a-d dimer in Fig. 2), and the other, through the second shortest-distance neighbors between the layers (a-c and b-d dimers in Fig. 2). For each scenario we identify the threshold interaction strength U_c,

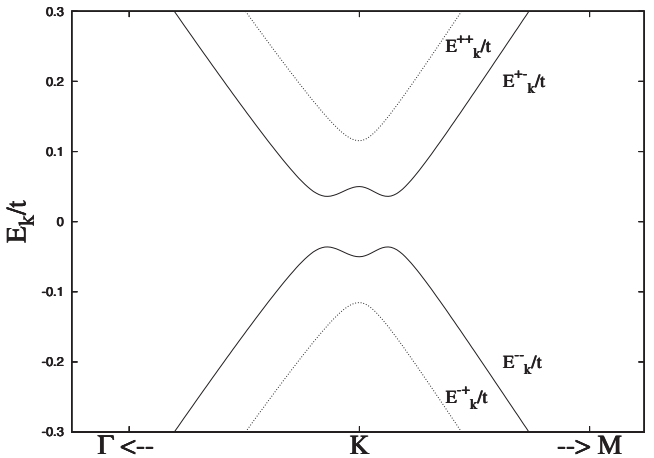

FIG. 1. Energy spectrum for the graphene bilayer with $t=2.9$ eV, $t_\perp/t=0.052$, and $V/t=0.05$. $E_k^{\pm-}/t$ in full line and $E_k^{\pm+}/t$ in dashed line. See text for definition of the energy branches labeled by $E_k^{\pm\pm}$.

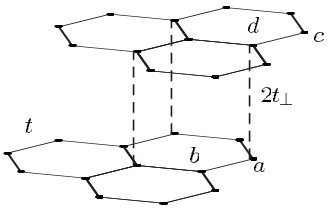

FIG. 2. Graphene bilayer (Bernal stacking). The *a-d* dimer is depicted as dashed lines.

and its dependence on the bias and the interlayer hopping parameter.

This work is divided into the following sequence. Section II describes the graphene bilayer and its model Hamiltonian, including the short-range Coulomb interaction across the layers. Two excitonic channels, which we will consider in this paper, are introduced. In the following two sections, each of these possibilities is examined in detail using the appropriate gap equations and their solutions. The work is summarized in Sec. V. Some of the technical aspects are summarized in the Appendix.

II. FORMULATION OF THE EXCITON PROBLEM

Graphene bilayer is a two honeycomb array stacked in a Bernal arrangement, as depicted in Fig. 2. In each layer the electrons can hop between nearest-neighbor carbon atoms through π orbitals with energy t, which is typically assumed to be at 2.9 eV. In a Bernal stacking, electrons are allowed to do interlayer hopping through the *a-d* dimers with the hopping energy given as $2t_\perp$ and with the $t_\perp/t$ given as approximately 0.052. Here a dimer is defined as the pair of carbon atoms from the adjacent layers stacked along the c axis.

In writing down the Hamiltonian appropriate for the graphene bilayer, we denote the electron operators for the two sublattices in the lower layer by a_i and b_i, and those in the upper layer by c_i and d_i. We assume a symmetric doping due to the external bias $\pm V$ with excess electrons and holes on the lower and upper graphene layers, respectively. We are interested in the formation of the same-spin electron-hole exciton here; hence the spin degree of freedom σ will be dropped. The Hamiltonian of the graphene bilayer, in the absence of the Coulomb interaction. reads

$$H_0 = -t\sum_{ij}(a_i^\dagger b_j + b_j^\dagger a_i + c_i^\dagger d_j + d_j^\dagger c_i) - 2t_\perp \sum_i (a_i^\dagger d_i + d_i^\dagger a_i) + V\sum_i (c_i^\dagger c_i + d_i^\dagger d_i - a_i^\dagger a_i - b_i^\dagger b_i). \quad (1)$$

After the diagonalization (derivation is given in Appendix A), Eq. (1) is transformed to

$$H_0 = k\sum (\alpha_k^\dagger \quad \beta_k^\dagger \quad \gamma_k^\dagger \quad \delta_k^\dagger)\begin{pmatrix} E_k^{++} & 0 & 0 & 0 \\ 0 & E_k^{+-} & 0 & 0 \\ 0 & 0 & E_k^{--} & 0 \\ 0 & 0 & 0 & E_k^{-+} \end{pmatrix}\begin{pmatrix} \alpha_k \\ \beta_k \\ \gamma_k \\ \delta_k \end{pmatrix}, \quad (2)$$

where $(\alpha_k, \beta_k, \gamma_k, \delta_k)$ now serve to define the eigenstates. The energy spectra depicted in Fig. 1 are the ones given by

$$E_k^{\pm\pm} = \pm\sqrt{\varepsilon_k^2 + 2t_\perp^2 + V^2 \pm 2\sqrt{t_\perp^4 + \varepsilon_k^2(t_\perp^2 + V^2)}}. \quad (3)$$

The bare kinetic energy ε_k within the monolayer reads $\varepsilon_k = t|\Sigma_{\alpha=1}^3 e^{ik.e_\alpha}|$, where e_α are the nearest-neighbor vectors of the graphene monolayer: $e_1=(1,0)$, $e_2=(-1/2,\sqrt{3}/2)$, and $e_3=(-1/2,-\sqrt{3}/2)$.

The two independent nodal points $K_{1(2)}$, where the bare electron spectrum ε_k vanishes, are chosen as $K_1=(0,\frac{4\pi}{3\sqrt{3}})$ $(K_2=-K_1)$ in the basis (e_x,e_y) in the Brillouin zone. The sum $\Sigma_\alpha e^{ik.e_\alpha}$ is approximately given by $-(3/2)(k_y-ik_x)$ near K_1 and by $(3/2)(k_y+ik_x)$ near K_2.

The bottom of the lower conduction band, E_k^{+-}, occurs at k points where $\varepsilon_k^2=(\varepsilon_k^2)_m=V^2(V^2+2t_\perp^2)/(V^2+t_\perp^2)$, with the energy $E_m=t_\perp V/\sqrt{t_\perp^2+V^2}$. The energy gap separating the valence and conduction bands is twice this value. The energy difference between the two conduction bands or the two valence bands is $\sqrt{V^2+2t_\perp^2}-V$ at $\varepsilon_k=0$ and $\sqrt{[4(V^4+t_\perp^4)+9V^2t_\perp^2]/(V^2+t_\perp^2)}-Vt_\perp/\sqrt{V^2+t_\perp^2}$ at $\varepsilon_k=(\varepsilon_k)_m$. These two quantities approach $t_\perp^2/V$ and $2V$, respectively, as $V/t_\perp\to\infty$. Generally, the presence of both interlayer hopping and the bias is essential in producing the gaps separating the various bands, as depicted in Fig. 1.

In describing the exciton formation, we propose to use the interlayer interaction truncated to the second-nearest neighbors as

$$V_C = U_1\sum_i n_{a,i}n_{d,i} + U_2\sum_{i\alpha}(n_{a,i}n_{c,i-e_\alpha} + n_{b,i}n_{d,i-e_\alpha}). \quad (4)$$

The local electronic densities are given by $n_{a,i}=a_i^\dagger a_i$, etc. The total Hamiltonian then reads $H=H_0+V_C$. The U_1 and U_2 terms are responsible for the exciton formation across the *a-d* dimer (nearest neighbor), and the *a-c* and *b-d* dimers (second-nearest neighbor), respectively.

At this point, several mean-field decoupling strategies present themselves. The average $\langle a_i^\dagger d_i\rangle$ might be a candidate order parameter for the exciton pairing but this quantity is nonzero even in the absence of any interlayer interaction, provided the interlayer tunneling $t_\perp$ remains nonzero. Only when $t_\perp=0$ does this average become the exact order parameter. Nevertheless, one can use the "difference" (to be quantified in the next section) of $\langle a_i^\dagger d_i\rangle$ obtained in the presence and absence of excitons as the order parameter. This is the strategy we adopt to discuss the *a-d* dimer exciton formation.

For the second-neighbor interaction, we could think of averages such as $\langle a_i^\dagger c_{i-e_\alpha}\rangle$ and $\langle b_i^\dagger d_{i-e_\alpha}\rangle$ as possible excitonic order parameters. Again, these averages are nonzero even in the absence of the interaction V_C. However, since averages $\langle a_i^\dagger c_{i-e_\alpha}\rangle$ for $\alpha=1,2,3$ are related by the Z_3 symmetry, one could form linear combinations $\Sigma_\alpha u_\alpha\langle a_i^\dagger c_{i-e_\alpha}\rangle$, which remains zero in the noninteracting case but becomes a nonzero value once the interaction U_2 is turned on and excitons are formed. The appropriate linear combination is easily identified. For the second-nearest-neighbor pairing, the excitonic order is directly related to the loss of Z_3 rotational symmetry of the lattice.

Finally, we assume that at low energy the main mechanism of the exciton formation is due to the hybridization of the upper valence (E_k^{+-}) and lower conduction bands (E_k^{--})

while the two outlying ones, E_k^{++} and E_k^{-+}, remain as spectators. Accordingly, the following reduced Hamiltonian may be used instead of Eq. (2):

$$H' = \sum_k E_k(\beta_k^\dagger \beta_k - \gamma_k^\dagger \gamma_k), \quad E_k = E_k^{+-} = -E_k^{--}. \tag{5}$$

Note that the two outlying bands are separated from the two inner ones by an energy difference that grows as V when $V/t_\perp$ is sufficiently large. The truncation scheme is expected to be valid when the bias V far exceeds the interlayer tunneling energy; a situation easily realized in tunable gate systems.[8,10] The interlayer interaction [Eq. (4)] will be truncated in the same subspace spanned by (β_k, γ_k). Such truncation greatly simplifies the algebra in subsequent discussions.

III. FIRST-NEIGHBOR EXCITON PAIRING

The first-neighbor interaction part reads

$$V_C(U_1) = U_1 \sum_i n_{a,i} n_{d,i} = U_1 \sum_{qkk'} a_{k+q}^\dagger a_k d_{k'-q}^\dagger d_{k'}. \tag{6}$$

According to our truncation scheme, the various operators can be expanded in terms of β_k and γ_k operators, corresponding to the lower conduction and upper valence bands, respectively;

$$a_k = U_{12}(k)\beta_k + U_{13}(k)\gamma_k,$$

$$d_k = U_{42}(k)\beta_k + U_{43}(k)\gamma_k.$$

The 4×4 unitary matrix U diagonalizing the Hamiltonian (1) (see Appendix A for a description of U) is used. The first-neighbor Coulomb interaction in the truncated space reads

$$\begin{aligned} V_C(U_1) = U_1 \sum_{qkk'} & [U_{12}^*(k+q)\beta_{k+q}^\dagger + U_{13}^*(k+q)\gamma_{k+q}^\dagger] \\ & \times [U_{12}(k)\beta_k + U_{13}(k)\gamma_k] \\ & \times [U_{42}^*(k'-q)\beta_{k'-q}^\dagger + U_{43}^*(k'-q)\gamma_{k'-q}^\dagger] \\ & \times [U_{42}(k')\beta_{k'} + U_{43}(k')\gamma_{k'}]. \end{aligned} \tag{7}$$

As our main concern is to explore the possibility of the excitonic order represented by nonzero $\langle \gamma_k^\dagger \beta_k \rangle$, we will only keep terms from Eq. (7) involving an even number of β and γ operators. In a Hartree-Fock approximation, the mean-field Hamiltonian, using the exciton order parameter for the $\beta-\gamma$ hybridization, can be written down as

$$V_C(U_1) = -\sum_k (\Delta_k \beta_k^\dagger \gamma_k + \Delta_k^* \gamma_k^\dagger \beta_k). \tag{8}$$

The exciton gap Δ_k is related to the exciton order parameter $\langle \gamma_k^\dagger \beta_k \rangle$ through

$$\begin{aligned} \Delta_k = & U_1 \left[\sum_q U_{12}(q) U_{43}^*(q) \langle \gamma_q^\dagger \beta_q \rangle \right] U_{12}^*(k) U_{43}(k) \\ & + U_1 \left[\sum_q U_{13}^*(q) U_{42}(q) \langle \gamma_q^\dagger \beta_q \rangle \right] U_{13}(k) U_{42}^*(k) \\ & - U_1 \left[\sum_q U_{42}(q) U_{43}^*(q) \langle \gamma_q^\dagger \beta_q \rangle \right] U_{12}^*(k) U_{13}(k) \\ & - U_1 \left[\sum_q U_{12}(q) U_{13}^*(q) \langle \gamma_q^\dagger \beta_q \rangle \right] U_{42}^*(k) U_{43}(k). \end{aligned} \tag{9}$$

Combining the kinetic part and the mean-field Coulomb interaction V_C, one obtains the full Hamiltonian

$$H = \sum_k E_k(\beta_k^\dagger \beta_k - \gamma_k^\dagger \gamma_k) - \sum_k (\Delta_k \beta_k^\dagger \gamma_k + \Delta_k^* \gamma_k^\dagger \beta_k). \tag{10}$$

The Hamiltonian (10) can be further diagonalized by the 2×2 unitary rotation

$$\begin{pmatrix} \beta_k \\ \gamma_k \end{pmatrix} = \begin{pmatrix} e^{i\gamma_k}\cos\theta_{5k} & e^{i\gamma_k}\sin\theta_{5k} \\ -\sin\theta_{5k} & \cos\theta_{5k} \end{pmatrix} \begin{pmatrix} B_k \\ C_k \end{pmatrix}, \tag{11}$$

with $e^{i\gamma_k} = \Delta_k/|\Delta_k|$, $\cos 2\theta_{5k} = E_k/\mathcal{E}_k$, and $\sin 2\theta_{5k} = |\Delta_k|/\mathcal{E}_k$. In terms of the eigenoperators B_k and C_k, and the eigenvalue $\mathcal{E}_k = \sqrt{E_k^2 + |\Delta_k|^2}$, the Hamiltonian (10) reads $H = \Sigma_k \mathcal{E}_k (B_k^\dagger B_k - C_k^\dagger C_k)$. The hybridization is given by

$$\langle \gamma_k^\dagger \beta_k \rangle = \frac{\Delta_k}{2\mathcal{E}_k} \tanh\left(\frac{\beta \mathcal{E}_k}{2} \right). \tag{12}$$

By inserting expressions of the unitary matrix elements [Eq. (A1)] and the hybridization [Eq. (12)] in Eq. (9), one readily finds that the phase of the gap function is dictated in the manner

$$\Delta_k = e^{-i\phi_k}|\Delta_k|, e^{i\phi_k} = \frac{\sum_\alpha e^{ik\cdot e_\alpha}}{\left|\sum_\alpha e^{ik\cdot e_\alpha}\right|}. \tag{13}$$

The phase factor in the excitonic gap has a winding of 2π around one Dirac point and -2π around the other. The total winding around the circumference of the full Brillouin zone is therefore zero.

A general connection between the phase singularity of the wave function and the singularities in the order parameters was considered in Ref. 22. This discussion can also be applied to excitonic order. In two dimensions, the topological structure discussed in Ref. 22 is defined as the total number of phase winding for the whole Brillouin zone, which in this case is zero. In fact, the phase winding around K_1 and K_2 in Eq. (13) can be removed by a gauge transformation,[23]

$$\beta_k' = \beta_k e^{i\phi_k}, \quad \gamma_k' = \gamma_k. \tag{14}$$

With this transformation, $\langle \gamma_k'^\dagger \beta_k' \rangle$ becomes real, and the phase vanishes at K_1 and K_2.

Taking out the phase, the gap [Eq. (9)] becomes

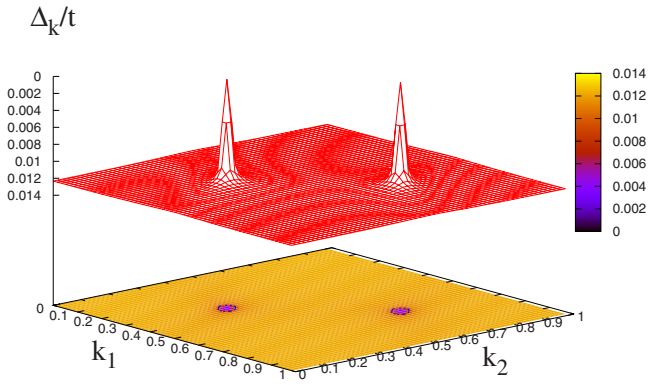

FIG. 3. (Color online) Exciton gap obtained from Eq. (15) at $T=0$. Here the parameters are: $t=2.9$ eV, $V/t=0.1$, $U_1/t=8.5$, and $t_\perp/t=0.052$ for a 60×60 lattice in the reciprocal space spanned by $k=k_1\mathbf{R}_1+k_2\mathbf{R}_2$. The reciprocal vectors $\mathbf{R}_1$ and $\mathbf{R}_2$ are defined by $\mathbf{R}_1=\frac{2\pi}{3}(1,\sqrt{3})$ and $\mathbf{R}_2=\frac{2\pi}{3}(-1,\sqrt{3})$.

$$|\Delta_k| = \frac{U_1}{16}\sum_p (1-\sin 2\theta_{2p})(1-\sin 2\theta_{2k}) \times[1+\cos(2\theta_{4p}-2\theta_{4k})]\frac{|\Delta_p|}{\mathcal{E}_p}\tanh\left(\frac{\beta\mathcal{E}_p}{2}\right). \quad (15)$$

The various factors are defined in Appendix A. The equation can be solved numerically for given values of U and V, and the interlayer hopping parameter $t_\perp$. The numerical solution of Eq. (15) is depicted in Fig. 3. Regarding the momentum dependence of the exciton gap, we see that it increases from zero at the nodal points to reach saturation far from K_1 and K_2.

Figure 4 shows the solution of Eq. (15) for a range of U_1 and various values of the bias V. At zero temperature a second-order phase transition of the exciton gap takes place with respect to the Coulomb interaction U_1 for each given bias V. This threshold value U_{1c}, at which excitons begin to form, is a function of V and is shown as a green line in Fig. 4. $U_{1c}(V)$ reaches a minimal value of $U_{1c}/t\simeq3.5$ for an "optimal" choice of the bias V_{1o} that is found at $V_{1o}/t\simeq1$.

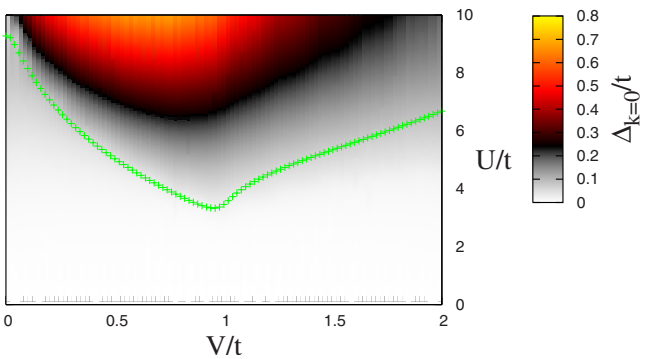

FIG. 4. (Color online) Zero temperature exciton gap magnitude $|\Delta_k|$ at $k=0$ (half way between K_1 and K_2), depending on the short-ranged Coulomb interaction U_1, and the bias V applied on the layers, obtained for 30×30 lattice with $t=2.9$ eV and $t_\perp/t=0.052$. The green line correspond to the threshold $U_{1c}(V)$ solution of Eq. (15) for a lattice size of 500×500 carbon atoms.

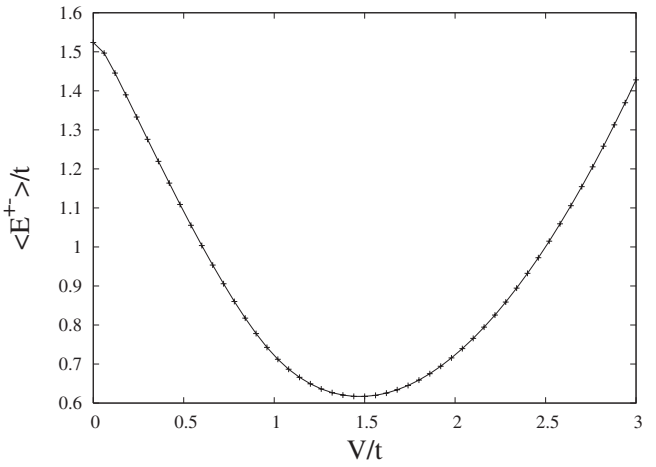

FIG. 5. Energy average $\langle E_k^{+-}\rangle$ depending on the bias V. The average of the energy is computed by summing E_k^{+-} over the whole Brillouin zone with $t=2.9$ eV and $t_\perp/t=0.052$.

Interestingly, the dependence on the bias $U_{1c}(V)$ appears to be related to the behavior of the exciton gap $\Delta_{k=0}$ obtained far away from the Dirac points at $k=0$, as shown in Fig. 4. The nonmonotonic dependence of the gap value on V is apparent. A similar behavior is observed in the conduction-valence-band energy gap, as exemplified in the Brillouin-zone average $\langle E_k^{+-}\rangle=\Sigma_{k\in BZ}E_k^{+-}$ shown in Fig. 5.

Using Eq. (15) we can deduce the dependence of $U_c(V)$ on the interlayer parameter $t_\perp$. As Fig. 6 shows, the threshold value decreases with $t_\perp$ and tends to zero as $t_\perp/t\to0$. Reducing the interlayer hopping parameter would reduce the threshold U_{1c} of the short-ranged Coulomb interaction above in which excitons can form. Intercalation of layers of nondoping and insulating atoms between the two carbon layers would reduce significantly the interlayer hopping parameter toward zero. The concomitant reduction in the Coulomb interaction U_1 with distance will be sufficiently slow compared to the exponential decay of $t_\perp$, so that the regime $U>U_c(V)$ can be attained for a range of bias around V_{1o}. Our analysis suggests that searching for ways to reduce the

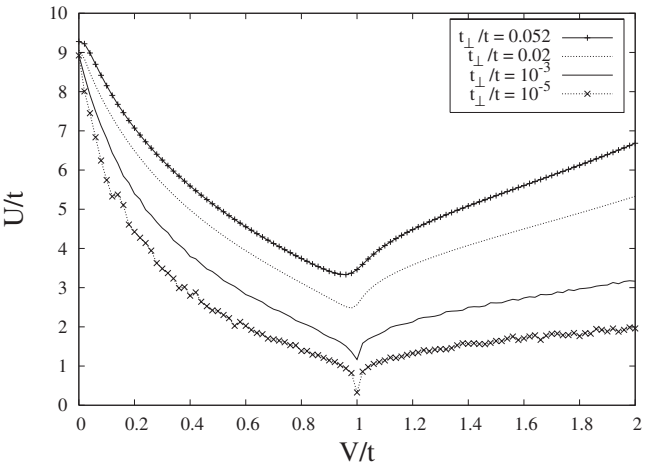

FIG. 6. Threshold U_{1c} depending on the bias V at zero temperature, $t=2.9$ eV, and various values of $t_\perp$.

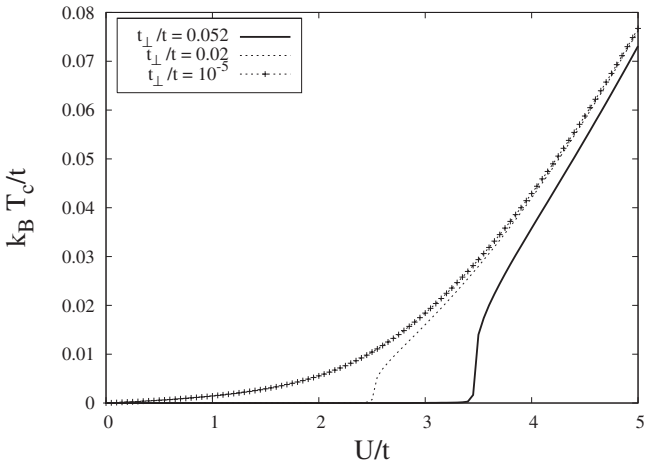

FIG. 7. Critical temperature T_c depending on the ratio U_1/t for several values of $t_\perp/t$. The critical temperature has been computed for 100×100 sublattice size and for the optimal value of the bias $V/t=1$. T_c tends to zero when $t_\perp/t\to0$.

interlayer hopping parameter experimentally would shed more light on the physics of exciton formation in graphene bilayer.

Finally, Fig. 7 depicts the behavior of the critical temperature T_c with respect to the Coulomb interaction U and for various hopping parameters $t_\perp$.

IV. SECOND-NEIGHBOR EXCITON PAIRING

Our approach in the previous section was based on the interaction with $U_2=0$. The average $\langle a_i^\dagger d_i\rangle$ read

$$\begin{aligned}\langle a_i^\dagger d_i\rangle &= \sum_k \langle a_k^\dagger d_k\rangle \\ &= \sum_k [U_{12}^*(k)U_{42}(k)\langle\beta_k^\dagger\beta_k\rangle + U_{13}^*(k)U_{43}(k)\langle\gamma_k^\dagger\gamma_k\rangle] \\ &\quad + \sum_k [U_{12}^*(k)U_{43}(k)\langle\beta_k^\dagger\gamma_k\rangle + U_{13}^*(k)U_{42}(k)\langle\gamma_k^\dagger\beta_k\rangle],\end{aligned} \tag{16}$$

in the scheme where the lowest and highest energy bands were truncated out. This average is nonzero even without the excitons at arbitrary temperature and is not a good measure of the possible phase transition in the model. Instead, we relied on the fact that $\langle\beta_k^\dagger\gamma_k\rangle$ is zero unless the excitons exist, and used this average as a measure of the excitonic order and excitonic phase transition in the model. Indeed this order parameter vanished at high enough temperature and/or weak enough coupling, allowing us to identify the critical points, and so forth.

In this section, we search for an excitonic order parameter defined in real space, which also vanishes identically for a nonexcitonic phase. The averages $\langle c_{i-e_\alpha}^\dagger a_i\rangle$ and $\langle d_{i-e_\alpha}^\dagger b_i\rangle$ are given by

$$\langle c_{i-e_\alpha}^\dagger a_i\rangle = \sum_k e^{ik\cdot e_\alpha}e^{-i\phi_k}f(k),$$

$$\langle d_{i-e_\alpha}^\dagger b_i\rangle = -\sum_k e^{ik\cdot e_\alpha}e^{-i\phi_k}f(k), \tag{17}$$

in the noninteracting limit [Eq. (2)]. The three unit vectors e_α were defined earlier as the difference of the nearest-neighbor positions in a given graphene layer. Here $f(k)$ is a function whose detailed form is unimportant to us. The combination $e^{-i\phi_k}f(k)$ is symmetric under the 120° rotation of the k vector, which in turn implies that $\langle c_{i-e_1}^\dagger a_i\rangle=\langle c_{i-e_2}^\dagger a_i\rangle=\langle c_{i-e_3}^\dagger a_i\rangle$, and $\langle d_{i-e_1}^\dagger b_i\rangle=\langle d_{i-e_2}^\dagger b_i\rangle=\langle d_{i-e_3}^\dagger b_i\rangle$.

This observation suggests a strategy for defining an appropriate order parameter. First define $h_{i\alpha}=c_{i-e_\alpha}^\dagger a_i$ and $g_{i\alpha}=d_{i-e_\alpha}^\dagger b_i$, then one can form the following linear combinations:

$$\chi_i^{(1)} = h_{i1} - \frac{1}{2}(h_{i2}+h_{i3}), \quad \Xi_i^{(1)} = g_{i1} - \frac{1}{2}(g_{i2}+g_{i3}),$$

$$\chi_i^{(2)} = h_{i2} - \frac{1}{2}(h_{i1}+h_{i3}), \quad \Xi_i^{(2)} = g_{i2} - \frac{1}{2}(g_{i1}+g_{i3}),$$

and

$$\chi^{(3)} = h_{i3} - \frac{1}{2}(h_{i1}+h_{i2}), \Xi_i^{(3)} = g_{i3} - \frac{1}{2}(g_{i1}+g_{i2}). \tag{18}$$

The operators $\chi_i^{(\beta)}$ and $\Xi_i^{(\beta)}$ have a zero average value in the nonexcitonic phase, $U_2=0$, due to the underlying Z_3 symmetry. In turn, nonzero value of one of the averages implies the Z_3 symmetry is spontaneously broken.

The short-ranged Coulomb interaction (4) with $U_1=0$ and $U_2\neq0$ will render the mean-field Hamiltonian

$$\begin{aligned}&-U_2\sum_{i,\alpha}(\langle a_i^\dagger c_{i-e_\alpha}\rangle c_{i-e_\alpha}^\dagger a_i + \text{h.c.}) \\ &\quad -U_2\sum_{i,\alpha}(\langle b_i^\dagger d_{i-e_\alpha}\rangle d_{i-e_\alpha}^\dagger b_i + h\,.\,c.).\end{aligned} \tag{19}$$

In terms of the new operator $\chi_i^{(\beta)}$ and $\Xi_i^{(\beta)}$ just defined, it can be recast in the form

$$\begin{aligned}V_C(U_2) = -\frac{4}{9}U_2\sum_i\Bigg[&\sum_\alpha(\langle\chi_i^{(\alpha)\dagger}\rangle\chi_i^{(\alpha)} + \langle\Xi_i^{(\alpha)\dagger}\rangle\Xi_i^{(\alpha)}) + \frac{3}{4}\langle h_{i,1}^\dagger \\ &+ h_{i,2}^\dagger + h_{i,3}^\dagger\rangle(h_{i,1}+h_{i,2}+h_{i,3}) + (h_{i\alpha}\to g_{i\alpha}) + \text{h.c.}\Bigg].\end{aligned} \tag{20}$$

The Coulomb interaction expressed in Eq. (20) is fully Z_3 symmetric (see Appendix B for the full expression of Eq. (20) in terms of the operator h_i only). We remark that the second line of Eq. (20) is irrelevant for the exciton formation and can be dropped.

Assuming translational invariance, we can take $\langle\chi_i^{(\beta)}\rangle=\langle\chi^{(\beta)}\rangle$ and $\langle\Xi_i^{(\beta)}\rangle=\langle\Xi^{(\beta)}\rangle$, and express the interaction as

$$V_C(U_2) = -\sum_k(\Theta_k\beta_k^\dagger\gamma_k + \Theta_k^*\gamma_k^\dagger\beta_k), \tag{21}$$

where Θ_k expresses the exciton gap. Using the total Hamiltonian $H=\Sigma_k E_k(\beta_k^\dagger\beta_k-\gamma_k^\dagger\gamma_k)-\Sigma_k(\Theta_k\beta_k^\dagger\gamma_k+\Theta_k^*\gamma_k^\dagger\beta_k)$, one can

derive the averages $\langle\chi^{(\beta)}\rangle$ and $\langle\Xi^{(\beta)}\rangle$ of the exciton order parameter from the self-consistent equations

$$\langle\chi^{(\beta)}\rangle = \frac{U_2}{9}\sum_k \tilde{\varphi}_k^{(\beta)}\cos^2(2\theta_{2k})\frac{1}{\mathcal{E}_k}\tanh\frac{\beta\mathcal{E}_k}{2} \times\left[i\cos^2(2\theta_{1k})\mathrm{Im}\left(\sum_{\beta'}\varphi_k^{(\beta')}\langle\chi^{(\beta')}\rangle\right) + \cos^2(2\theta_{4k})\mathrm{Re}\left(\sum_{\beta}\varphi_k^{(\beta')}\langle\chi^{(\beta')}\rangle\right)\right], \quad (22)$$

for $\beta=\{1,2,3\}$. The averages $\langle\Xi^{(\beta)}\rangle$ are related to $\langle\chi^{(\beta)}\rangle$ by the simple relation $\langle\Xi^{(\beta)}\rangle=-\langle\chi^{(\beta)}\rangle$ for any β. We defined

$$\varphi_k^{(1)} = e^{i\phi_k}\left[e^{ik.e_1} - \frac{1}{2}(e^{ik.e_2}+e^{ik.e_3})\right],$$

$$\tilde{\varphi}_k^{(1)} = e^{-i\phi_k}\left[e^{ik.e_1} - \frac{1}{2}(e^{ik.e_2}+e^{ik.e_3})\right], \quad (23)$$

and the Z_3 symmetric counterparts $\varphi_k^{(2)}$, $\varphi_k^{(3)}$, $\tilde{\varphi}_k^{(2)}$, and $\tilde{\varphi}_k^{(3)}$ accordingly. The energy of the quasiparticles reads $\mathcal{E}_k=\sqrt{E_k^2+|\Theta_k|^2}$ and the exciton gap is given by

$$e^{i\phi_k}\Theta_k = \frac{U_2}{9}\cos(2\theta_{2k})\left[\cos(2\theta_{1k})4i\ \mathrm{Im}\left(\sum_{\beta}\varphi_k^{(\beta)}\langle\chi^{\beta}\rangle\right) + \cos(2\theta_{4k})4\ \mathrm{Re}\left(\sum_{\beta}\varphi_k^{(\beta)}\langle\chi^{\beta}\rangle\right)\right]. \quad (24)$$

The system of self-consistent Eqs. (22) admits an ensemble of solutions, all obeying $\Sigma_\beta\langle\chi^{(\beta)}\rangle=0$. As it turns out, the numerical solution always follows the condition that two of the $|\chi^{(\alpha)}|$ are the same and different from the third. Furthermore, the phases of the two equal-amplitude bonds can be made equal through phase redefinition of the operators and we can choose, for instance, $\chi^{(2)}=\chi^{(3)}\neq\chi^{(1)}$ without loss of generality. The other choices are related by Z_3 permutation.

We will now exclusively consider the configuration $\langle\chi^{(1)}\rangle\neq\langle\chi^{(2)}\rangle=\langle\chi^{(3)}\rangle$, where, due to $\Sigma_\beta\chi^{(\beta)}=0$, the following relation holds:

$$\langle\chi^{(1)}\rangle = -2\langle\chi^{(2)}\rangle = -2\langle\chi^{(3)}\rangle. \quad (25)$$

Introducing relation (25) into Eq. (22), one gets a single self-consistent equation of the exciton instability,

$$\langle\chi^{(1)}\rangle = \frac{U_2}{9}\sum_k \tilde{\varphi}_k^{(1)}\cos^2(2\theta_{2k})\frac{1}{\mathcal{E}_k}\tanh\frac{\beta\mathcal{E}_k}{2} \times\left\{i\cos^2(2\theta_{1k})\ \mathrm{Im}\left[\left(\varphi_k^{(1)}-\frac{1}{2}(\varphi_k^{(2)}+\varphi_k^{(3)})\right)\langle\chi^{(1)}\rangle\right] + \cos^2(2\theta_{4k})\mathrm{Re}\left[\left(\varphi_k^{(1)}-\frac{1}{2}(\varphi_k^{(2)}+\varphi_k^{(3)})\right)\langle\chi^{(1)}\rangle\right]\right\}. \quad (26)$$

Solution of this can be used to generate the exciton gap Θ_k using Eq. (24).

Figure 8 represents the amplitude of the exciton gap $|\Theta_k|$ over the whole Brillouin zone of the graphene bilayer. The exciton gap vanishes at the Dirac nodal points K_1 and K_2, as well as for a wave vector $\mathbf{k}=\frac{1}{2}(\mathbf{R}_1+\mathbf{R}_2)$, where $\mathbf{R}_1=\frac{2\pi}{3}(1,\sqrt{3})$ and $\mathbf{R}_2=\frac{2\pi}{3}(-1,\sqrt{3})$. The vanishing of the exciton amplitude at the point $\frac{1}{2}(\mathbf{R}_1+\mathbf{R}_2)$ marks the breaking of the Z_3 symmetry (Fig. 9).

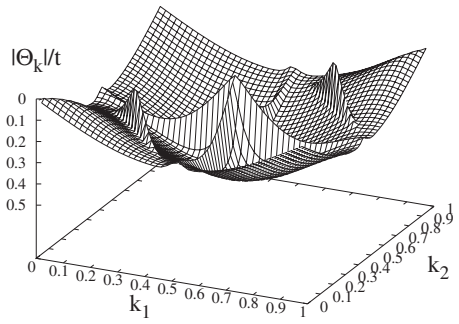

FIG. 8. The exciton gap amplitude $|\Theta_k|/t$ is plotted over the whole Brillouin zone of the graphene bilayer. The parameters are $t_\perp/t=0.052$ and $V/t=1$. The Coulomb interaction $U_1=0$ and we have chosen an arbitrary value $U_2/t=3$ for a 50×50 lattice in the reciprocal space spanned by $k=k_1\mathbf{R}_1+k_2\mathbf{R}_2$.

With Eq. (26), one can derive the threshold Coulomb interaction strength, which reads

$$\frac{1}{U_{2c}} = \frac{1}{9}\sum_k \cos^2(2\theta_{2k})\frac{1}{E_k}\tanh\frac{\beta E_k}{2} \times\left[\cos^2(2\theta_{4k})\mathrm{Re}(\tilde{\varphi}_k^{(1)})\mathrm{Re}\left(\varphi_k^{(1)}-\frac{1}{2}(\varphi_k^{(2)}+\varphi_k^{(3)})\right) - \cos^2(2\theta_{1k})\mathrm{Im}(\tilde{\varphi}_k^{(1)})\mathrm{Im}\left(\varphi_k^{(1)}-\frac{1}{2}(\varphi_k^{(2)}+\varphi_k^{(3)})\right)\right]. \quad (27)$$

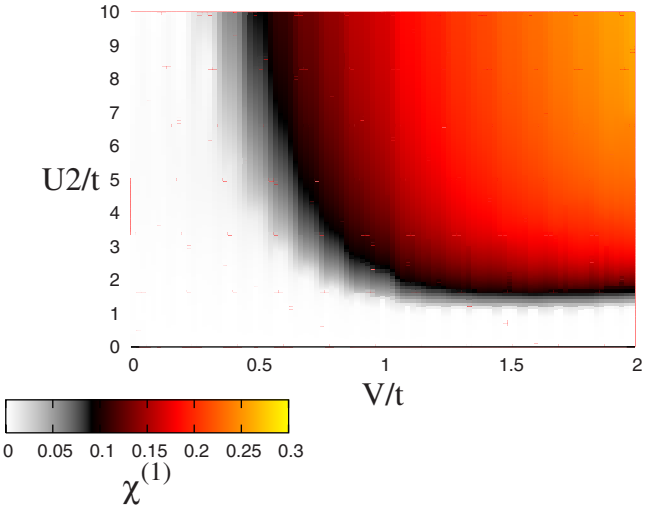

FIG. 9. (Color online) Contour of the amplitude of the exciton average $\langle\chi^{(1)}\rangle$ in the configuration for which $\langle\chi^{(1)}\rangle\neq\langle\chi^{(2)}\rangle\neq\langle\chi^{(3)}\rangle$. Here $t=2.9$ eV, $t_\perp/t=0.052$, $V/t=1$, and we used a sublattice of 30×30 carbon atoms.

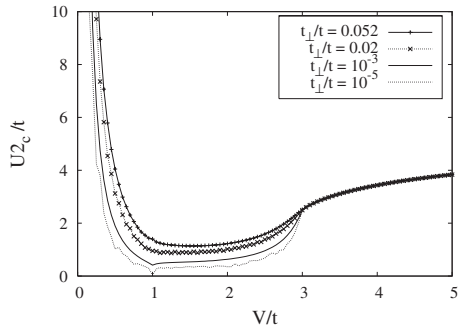

FIG. 10. Coulomb threshold U_{2c} depending on the bias V for various interlayer hopping parameters $t_\perp$. We used $t=2.9$ eV and sublattices of 50×50–1200×1200 carbon atoms.

Figure 10 shows the variation of U_{c2} with V/t for various values of $t_\perp/t$. The similarity of this plot to Fig. 6 is obvious. As for the case treating the Coulomb interaction on dimer *a-d*, we see that there is an optimal value $V_{2o}/t\simeq 1$, for which the threshold U_{2c} is minimal. Moreover as the interlayer parameter $t_\perp$ is decreased (by intercalation of insulating and nondoping atoms), the Coulomb threshold decreases.

The critical temperature T_c follows from

$$1 = \frac{U_2}{9}\sum_k \cos^2(2\theta_{2k})\frac{1}{E_k}\tanh\frac{E_k}{2k_BT_c} \times \left[\cos^2(2\theta_{4k})\mathrm{Re}(\tilde{\varphi}_k^{(1)})\mathrm{Re}\left(\varphi_k^{(1)} - \frac{1}{2}(\varphi_k^{(2)} + \varphi_k^{(3)})\right) - \cos^2(2\theta_{1k})\mathrm{Im}(\tilde{\varphi}_k^{(1)})\mathrm{Im}\left(\varphi_k^{(1)} - \frac{1}{2}(\varphi_k^{(2)} + \varphi_k^{(3)})\right)\right]. \tag{28}$$

Figure 11 depicts the variation of the critical temperature with respect to the Coulomb interaction and for various values of the interlayer hopping parameter $t_\perp$. As for the dimer *a-d* Coulomb interaction, exciton are formed at higher temperatures for smaller $t_\perp/t$.

The behavior observed in this section are in good agreement with the behavior of the critical temperature T_c and the Coulomb threshold U_{1c}, observed in the case treating the Coulomb interaction U_1 on dimer *a-d*. However the Coulomb threshold U_{2c} is smaller than the threshold U_{c1}. For $t=2.9$ eV and $t_\perp/t=0.052$ at the optimal value of the bias $V_o/t\simeq 1$, one gets $U_{1c}/t\simeq 3.5$, compared to $U_{2c}/t\simeq 1.5$.

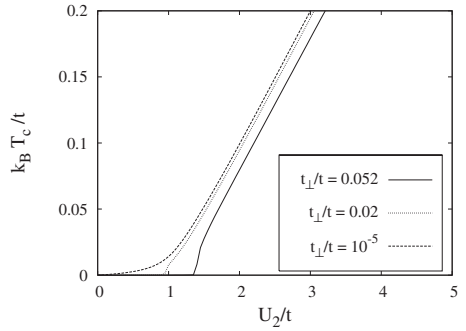

FIG. 11. Critical temperature for various Coulomb interaction and different interlayer hopping parameters $t_\perp$, as given in Eq. (28). Here $t=2.9$ eV, $t_\perp/t=0.052$, $V/t=1$ and we used a sublattice with 50×50 carbon atoms. Note the similarity to T_c plot in Fig. 7.

V. CONCLUSIONS

The graphene bilayer system was considered with a short-ranged Coulomb interaction acting between the nearest and next-nearest carbon sites in a Bernal stacking scheme of two carbon layers. The short-ranged Coulomb interaction was introduced for both nearest (U_1 for *a-d* dimer) and second-nearest (U_2 for *a-c* and *b-d* dimers) neighbors between the two layers.

For a given bias V or electron-hole imbalance between the layers, a critical Coulomb interaction strength exists above where the excitons form. For the first-neighbor *a-d* dimer interaction, the critical strength is $U_c/t\simeq 3.5$ for a bias $V/t\simeq 1$. The threshold becomes smaller in the case of only the second-neighbor Coulomb interaction and approximately equal to $U_{2c}/t\simeq 1.5$ at $V/t\simeq 1$. Hence, doping by equal and opposite charges of the bilayer system with the voltage difference applied perpendicular to the bilayer can control the excitonic properties of the graphene bilayer in a nontrivial way. The optimal value of the bias V (which gives rise to the least threshold value U_c) was found to be $V_o/t\simeq 1$. This nonmonotonic dependence on the bias reflects the dependence of the energy gap between the conduction and valence band graphene bilayers on the same quantity.

Moreover, we showed that reducing the interlayer hopping parameter $t_\perp\to 0$ reduces the threshold near the optimal bias $U_c(V_o)$ to zero. We suggest that intercalation of nondoping and insulating atomic layers between the carbon layers could reduce significantly $t_\perp$ in such a way that the screened Coulomb interaction U obeys the condition $U>U_c$ (for bias around the optimal value V_o), and excitons could form. It thus seems possible that the formation of the exciton gap can be controlled experimentally by both applying an electric field perpendicular to the graphene bilayer and tuning the interlayer hopping.[10,24]

The next step in the study of the exciton formation would lie in considering the long-ranged Coulomb interaction between the two carbon layers. We conjecture that treating the long-range Coulomb interaction might reduce the threshold U_c toward a reasonable value accessible by real graphene bilayer systems.[8,25]

ACKNOWLEDGMENTS

The authors are grateful to Shuichi Murakami and Cheol Hwan Park for their comments on the manuscript.

APPENDIX A: DIAGONALIZATION OF THE HAMILTONIAN

In the momentum space the bilayer Hamiltonian (1) reads

$$H = -\sum_k \psi_k^\dagger H_k \psi_k,$$

where $\psi_k^T=(a_k b_k c_k d_k)$ and

$$H_k = \begin{pmatrix} V & t\sum_\alpha e^{ik\cdot e_\alpha} & 0 & 2t_\perp \\ t\sum_\alpha e^{-ik\cdot e_\alpha} & V & 0 & 0 \\ 0 & 0 & -V & t\sum_\alpha e^{ik\cdot e_\alpha} \\ 2t_\perp & 0 & t\sum_\alpha e^{-ik\cdot e_\alpha} & -V \end{pmatrix}.$$

The unitary matrix diagonalizing the Hamiltonian is given by a string of matrices,

$$U_k = U_{0k}U_{1k}U_{2k}U_{3k},$$

$$U_{0k} = \frac{1}{\sqrt{2}}\begin{pmatrix} e^{i\phi_k} & e^{i\phi_k} & 0 & 0 \\ 1 & -1 & 0 & 0 \\ 0 & 0 & e^{i\phi_k} & e^{i\phi_k} \\ 0 & 0 & 1 & -1 \end{pmatrix},$$

and

$$e^{i\phi_k} = \mathrm{ph}\left(\alpha\sum e^{ik\cdot e_\alpha}\right).$$

After diagonalizing with U_{0k}, one has

$$U_{0k}^\dagger H_k U_{0k} = \begin{pmatrix} V+\varepsilon_k & 0 & t_\perp e^{-i\phi_k} & -t_\perp e^{-i\phi_k} \\ 0 & V-\varepsilon_k & t_\perp e^{-i\phi_k} & -t_\perp e^{-i\phi_k} \\ t_\perp e^{i\phi_k} & t_\perp e^{i\phi_k} & -V+\varepsilon_k & 0 \\ -t_\perp e^{i\phi_k} & -t_\perp e^{i\phi_k} & 0 & -V-\varepsilon_k \end{pmatrix}.$$

The second rotation is implemented by

$$U_{1k} = \begin{pmatrix} \cos\theta_1 & 0 & -\sin\theta_1 e^{-i\phi_k} & 0 \\ 0 & \cos\theta_1 & 0 & \sin\theta_1 e^{-i\phi_k} \\ \sin\theta_1 e^{i\phi_k} & 0 & \cos\theta_1 & 0 \\ 0 & -\sin\theta_1 e^{i\phi_k} & 0 & \cos\theta_1 \end{pmatrix},$$

$$\cos 2\theta_1 = \frac{V}{\sqrt{V^2+t_\perp^2}}, \sin 2\theta_1 = \frac{t_\perp}{\sqrt{V^2+t_\perp^2}}.$$

After diagonalizing with U_{1k} one has

$$U_{1k}^\dagger U_{0k}^\dagger H_k U_{0k} U_{1k} = \begin{pmatrix} \varepsilon_k+\lambda & t_\perp^2/\lambda & 0 & -e^{-i\phi_k}Vt_\perp/\lambda \\ t_\perp^2/\lambda & -\varepsilon_k+\lambda & e^{-i\phi_k}Vt_\perp/\lambda & 0 \\ 0 & e^{i\phi_k}Vt_\perp/\lambda & \varepsilon_k-\lambda & t_\perp^2/\lambda \\ -e^{i\phi_k}Vt_\perp/\lambda & 0 & t_\perp^2/\lambda & -\varepsilon_k-\lambda \end{pmatrix},$$

where $\lambda=\sqrt{V^2+t_\perp^2}$. The next step in the diagonalization is affected by

$$U_{2k} = \begin{pmatrix} \cos\theta_{2k} & -\sin\theta_{2k} & 0 & 0 \\ \sin\theta_{2k} & \cos\theta_{2k} & 0 & 0 \\ 0 & 0 & \cos\theta_{2k} & -\sin\theta_{2k} \\ 0 & 0 & \sin\theta_{2k} & \cos\theta_{2k} \end{pmatrix},$$

$$\cos 2\theta_{2k} = \frac{\varepsilon_k\lambda}{\sqrt{t_\perp^4+\varepsilon_k^2\lambda^2}}, \quad \sin 2\theta_{2k} = \frac{t_\perp^2}{\sqrt{t_\perp^4+\varepsilon_k^2\lambda^2}}.$$

After diagonalizing with U_{2k}, one has

$$U_{2k}^\dagger U_{1k}^\dagger U_{0k}^\dagger H_k U_{0k} U_{1k} U_{2k} = \begin{pmatrix} \lambda+\xi_k/\lambda & 0 & 0 & -e^{-i\phi_k}Vt_\perp/\lambda \\ 0 & \lambda-\xi_k/\lambda & e^{-i\phi_k}Vt_\perp/\lambda & 0 \\ 0 & e^{i\phi_k}Vt_\perp/\lambda & -\lambda+\xi_k/\lambda & 0 \\ -e^{i\phi_k}Vt_\perp/\lambda & 0 & 0 & -\lambda-\xi_k/\lambda \end{pmatrix},$$

where $\xi_k=\sqrt{\varepsilon_k^2\lambda^2+t_\perp^4}$. The final step in the diagonalization is given by

$$U_{3k} = \begin{pmatrix} \cos\theta_{3k} & 0 & 0 & \sin\theta_{3k}e^{-i\phi_k} \\ 0 & \cos\theta_{4k} & -\sin\theta_{4k}e^{-i\phi_k} & 0 \\ 0 & \sin\theta_{4k}e^{i\phi_k} & \cos\theta_{4k} & 0 \\ -\sin\theta_{3k}e^{i\phi_k} & 0 & 0 & \cos\theta_{3k} \end{pmatrix},$$

$$\cos 2\theta_{3k} = \frac{\lambda^2+\xi_k}{\sqrt{V^2t_\perp^2+(\lambda^2+\xi_k)^2}}, \quad \sin 2\theta_{3k} = \frac{Vt_\perp}{\sqrt{V^2t_\perp^2+(\lambda^2+\xi_k)^2}}$$

$$\cos 2\theta_{4k} = \frac{\lambda^2-\xi_k}{\sqrt{V^2t_\perp^2+(\lambda^2-\xi_k)^2}}, \quad \sin 2\theta_{4k} = \frac{Vt_\perp}{\sqrt{V^2t_\perp^2+(\lambda^2-\xi_k)^2}}.$$

After diagonalizing with U_{3k}, one has

$$U_{3k}^{\dagger}U_{2k}^{\dagger}U_{1k}^{\dagger}U_{0k}^{\dagger}H_kU_{0k}U_{1k}U_{2k}U_{3k}=\begin{pmatrix} E_k^{++} & 0 & 0 & 0 \\ 0 & E_k^{+-} & 0 & 0 \\ 0 & 0 & E_k^{--} & 0 \\ 0 & 0 & 0 & E_k^{-+} \end{pmatrix},$$

where $E_k^{\pm\pm}=\pm\sqrt{\varepsilon_k^2+\lambda^2+t_\perp^2\pm 2\xi_k}$. Combining the four unitary matrices into one, $U_k=U_{0k}U_{1k}U_{2k}U_{3k}$, the eigenoperators are obtained as

$$\begin{pmatrix} a_k \\ b_k \\ c_k \\ d_k \end{pmatrix}=U_k\begin{pmatrix} \alpha_k \\ \beta_k \\ \gamma_k \\ \delta_k \end{pmatrix}.$$

The unitary matrix U leads to the following expressions needed in the evaluation of the exciton gap [Eq. (9)],

$$U_{12}(k)U_{43}^{*}(k)=\frac{1}{4}e^{i\phi_k}(1-\sin 2\theta_{2k})[1+\cos(2\theta_1+2\theta_{4k})],$$

$$U_{42}(k)U_{13}^{*}(k)=-\frac{1}{4}e^{i\phi_k}(1-\sin 2\theta_{2k})[1-\cos(2\theta_1+2\theta_{4k})],$$

$$U_{42}(k)U_{43}^{*}(k)=\frac{1}{4}e^{i\phi_k}(1-\sin 2\theta_{2k})\sin(2\theta_1+2\theta_{4k}),$$

and

$$U_{12}(k)U_{13}^{*}(k)=-\frac{1}{4}e^{i\phi_k}(1-\sin 2\theta_{2k})\sin(2\theta_1+2\theta_{4k}). \tag{A1}$$

APPENDIX B: SECOND-NEIGHBOR COULOMB INTERACTION

The second-neighbor mean-field Coulomb interaction with $U_1=0$ can be rewritten in terms of the operator $h_i=c_i^{\dagger}a_i$ and $g_i=d_i^{\dagger}b_i$ in the following form

$$\begin{aligned} V_C=-\frac{4}{9}U_2\sum_i\Bigg[&\left(h_{i,1}^{\dagger}-\frac{1}{2}(h_{i,2}^{\dagger}+h_{i,3}^{\dagger})\right)\left(h_{i,1}-\frac{1}{2}(h_{i,2}+h_{i,3})\right) \\ &+\left(h_{i,2}^{\dagger}-\frac{1}{2}(h_{i,1}^{\dagger}+h_{i,3}^{\dagger})\right)\left(h_{i,2}-\frac{1}{2}(h_{i,1}+h_{i,3})\right) \\ &+\left(h_{i,3}^{\dagger}-\frac{1}{2}(h_{i,1}^{\dagger}+h_{i,2}^{\dagger})\right)\left(h_{i,3}-\frac{1}{2}(h_{i,1}+h_{i,2})\right) \\ &+\frac{3}{4}\langle h_{i,1}^{\dagger}+h_{i,2}^{\dagger}+h_{i,3}^{\dagger}\rangle(h_{i,1}+h_{i,2}+h_{i,3})+\text{h.c.}\Bigg]+h\rightarrow g. \end{aligned} \tag{B1}$$

*raoul.dillenschneider@physik.uni-augsburg.de
†hanjh@skku.edu

[1] K. S. Novoselov, A. K. Geim, S. V. Morozov, D. Jiang, M. I. Katsnelson, I. V. Grigorieva, S. V. Dubonos, and A. A. Firsov, Nature (London) **438**, 197 (2005).
[2] K. S. Novoselov, E. McCann, S. V. Morozov, V. I. Falko, M. I. Katsnelson, U. Zeitler, D. Jiang, F. Schedin, and A. K. Geim, Nat. Phys. **2**, 177 (2006).
[3] Y. Zhang, Y.-W. Tan, H. L. Stormer, and P. Kim, Nature (London) **438**, 201 (2005).
[4] A. K. Geim and K. S. Novoselov, Nat. Mater. **6**, 183 (2007).
[5] E. McCann and V. I. Fal'ko, Phys. Rev. Lett. **96**, 086805 (2006).
[6] D. S. L. Abergel and Vladimi I. Fal'ko, Phys. Rev. B **75**, 155430 (2007).
[7] G. W. Semenoff, Phys. Rev. Lett. **53**, 2449 (1984).
[8] E. V. Castro, K. S. Novoselov, S. V. Morozov, N. M. R. Peres, J. M. B. Lopes dos Santos, J. Nilsson, F. Guinea, A. K. Geim, and A. H. Castro Neto, Phys. Rev. Lett. **99**, 216802 (2007).
[9] L. M. Malard, J. Nilsson, D. C. Elias, J. C. Brant, F. Plentz, E. S. Alves, A. H. Castro Neto, and M. A. Pimenta, Phys. Rev. B **76**, 201401 (2007).
[10] J. B. Oostinga, H. B. Heersche, X. Liu, A. F. Morpurgo, and L. M. K. Vandersypen, Nat. Mater. **7**, 151 (2007).
[11] A. V. Balatsky, Y. N. Joglekar, and P. B. Littlewood, Phys. Rev. Lett. **93**, 266801 (2004).
[12] Jung Hoon Han and Chenglong Jia, Phys. Rev. B **74**, 075105 (2006).
[13] T. C. Ribeiro, A. Seidel, J. H. Han, and D.-H. Lee, Europhys. Lett. **76**, 891 (2006).
[14] B. I. Halperin and T. M. Rice, Rev. Mod. Phys. **40**, 755 (1968).
[15] D. V. Khveshchenko, Phys. Rev. Lett. **87**, 206401 (2001).
[16] D. V. Khveshchenko and W. F. Shively, Phys. Rev. B **73**, 115104 (2006).
[17] T. W. Appelquist, M. Bowick, D. Karabali, and L. C. R. Wijewardhana, Phys. Rev. D **33**, 3704 (1986).
[18] H. Leal and D. V. Khveshchenko, Nucl. Phys. B **687**, 323 (2004).
[19] V. P. Gusynin, V. A. Miransky, and I. A. Shovkovy, Phys. Rev. Lett. **73**, 3499 (1994).
[20] E. V. Gorbar, V. P. Gusynin, V. A. Miransky, and I. A. Shovkovy, Phys. Rev. B **66**, 045108 (2002).
[21] J. Nilsson, A. H. Castro Neto, F. Guinea, and N. M. R. Peres, Phys. Rev. Lett. **97**, 266801 (2006).
[22] S. Murakami and N. Nagaosa, Phys. Rev. Lett. **90**, 057002 (2003).
[23] We are particularly grateful to Shuichi Murakami for pointing out this gauge transformation and the removal of the phase factor in the gap function thereafter.
[24] H. Min, B. Sahu, S. K. Banerjee, and A. H. MacDonald, Phys. Rev. B **75**, 155115 (2007).
[25] T. Ohta, A. Bostwick, T. Seyller, K. Horn, and E. Rotenberg, Science **313**, 951 (2006).